




Effects of chromium on the morphology and mechanical properties of Fe₂B intermetallic in Fe-3.0B alloy

Yongxin Jian¹ , Zhifu Huang^{1,*}, Jiandong Xing¹, and Yimin Gao¹

¹ State Key Laboratory for Mechanical Behavior of Materials, School of Materials Science and Engineering, Xi'an Jiaotong University, No. 28, Xianning West Road, Xi'an, Shaanxi Province 710049, People's Republic of China

Received: 20 May 2017

Accepted: 15 December 2017

Published online:

2 January 2018

© Springer Science+Business Media, LLC, part of Springer Nature 2017

ABSTRACT

In this work, the effects of chromium addition on the morphology and mechanical properties of Fe₂B in Fe-3.0B alloy have been systematically investigated by a combination of experimental observations and the first-principles calculations. The results indicate that, with chromium addition in Fe-3.0B alloy ranging from 0 to 2.5 wt%, the average grain size of the boride firstly decreases and then increases slightly, mainly attributed to the volume fraction of coarse block boride. The nanoindentation hardness H of the boride remains almost constant while the elastic modulus E_r firstly drops and then rises. Accordingly, the H/E_r of the boride achieves a peak value at the chromium addition of 2.0 wt%, where the highest toughness is obtained. High-resolution transmission electron microscopy (HRTEM) observation demonstrates that the lattice of borides evolves from tetragonal to orthorhombic ((Fe, Cr)₂B) after chromium addition, in good accordance with the calculation results. During the lattice evolution, a shrinkage of B–B bond along [002] direction is simultaneously revealed. The inherently weak B–B bond can be strengthened, which improves fracture toughness of Fe₂B.

Introduction

Economic losses caused by the abrasion and corrosion are considerable in the mechanical components and structures. Exploring superior wear-resistant and corrosion-resistant materials has been the permanently hot topic for researchers in the field of material science [1–7].

Cast alloys with high boron and low carbon (Fe–B alloys), consisting of metallic matrix (such as ferrite or pearlite) and hard boride (Fe₂B), show two principal advantages over the most of wear and corrosion-resistant materials. On the one hand, the production cost for Fe–B alloys, e.g. raw materials, is relatively economical compared with traditional high-chromium cast iron. On the other hand, it is feasible to tailor the content of the boride and carbon

Address correspondence to E-mail: zhifuhuangxjtu@163.com

in the metallic matrix so as to independently control the hardness of the alloy and metallic matrix based on the low solubility of boron in austenite and ferrite and poor dissolution ability of carbon into the crystal of Fe₂B [8]. Therefore, Fe–B alloy has been highly addressed as a potential candidate for wear- and corrosion-resistant material [9–20].

In the past few decades, modifying the microstructure and improving the wear, corrosion resistance have been the key goal in researches related to Fe–B alloys. Initially, Yi [19] and Zhang [18] found that Fe–B alloy exhibited comparable wear resistance with high-chromium cast iron. Subsequently, Ma [17] and Wang [16] investigated the erosion-corrosion behavior of Fe-3.5B alloy at elevated temperature in zinc melt, indicating that orientation and lamellar spacing of Fe₂B had significant influence on the erosion-corrosion behavior of the alloy. By studying the microstructure, mechanical properties and oxidation behavior of Fe–B–C–Cr–Al alloys [14, 15], Lv et al. reported that Fe–3.08 wt% B alloy presented excellent oxidation resistance attributed to the inhibiting effect of the boride. Additionally, the author has also investigated the effects of chromium addition on the abrasive wear behaviors of Fe-3.0 B alloy in previous work [10, 12]. To sum up, all preceding studies draw an accordant conclusion that the hard boride (Fe₂B) plays a dominant role in the corrosion-, wear- and oxidation-resistant performance.

In spite of the advantages of Fe–B alloys, however, Fe₂B is in fact intrinsically brittle due to the weak B–B bond along [002] direction [21]. The lack of toughness of Fe₂B is a well-known bottleneck that limits the widespread engineering application of Fe–B alloy. Nevertheless, very few works explored the effective ways to improve the toughness of Fe₂B directly and shed light on the intrinsic mechanism. In this case, this work is to investigate the effects of chromium on the morphology and mechanical properties of Fe₂B in Fe–3.0B alloy. The morphological evolution of Fe₂B is quantitatively analyzed as a function of chromium content. Mechanical properties of Fe₂B, especially the toughness, are systematically studied with the aid of nanoindentation technique. Furthermore, HRTEM and the first-principles calculation have been implemented to explain the underlying mechanism.

Materials and methods

Sample preparation

In this work, Fe-3.0B alloys with a series of chromium content (0, 1.0, 1.5, 2.0 and 2.5 wt%) were melt in a medium frequency induction furnace. To acquire the heat-treated microstructure, the five cast ingots were austenitized at 980°C and then quenched in oil. Subsequently, all samples were tempered at 220°C to eliminate the quenching stress. The chemical compositions of all samples are shown in Table 1.

The standard specimens for metallography and mechanical properties tests were sectioned from the lower part of the ingots using the electrical discharge machining (EDM) **equipment**. Specimens were carefully polished to a mirror finish using abrasive papers with varying meshes. To reveal the microstructure, the specimen was etched by 4 vol% nital.

Microstructure examination

Microstructure observation was conducted utilizing an optical microscopy (LEICA DMI 5000 M, OM) and a scanning electron microscopy (VEGAIIXMUINCA, SEM). Electron probe microanalysis (JXA-8230, EPMA) was used to analyze the chromium distribution in the alloy.

A high-resolution transmission electron microscope (JEM-2000F, HRTEM) was used to identify the distinct phases in the alloy. The experimental results were analyzed with the aid of the professional processing software (Gantan Digital Micrograph). The standard thin foil specimen for TEM examination was prepared by the initial mechanical grind and subsequent twin-jet electropolishing in solution of 5 vol% perchloric acid and 95% alcohol.

Table 1 Chemical compositions of Fe-3.0B alloys with different chromium additions (wt%)

Sample	C	B	Cr	Mn	Si	Fe
0Cr	0.28	3.01	0	0.50	0.61	Bal.
1.0Cr	0.30	2.95	0.97	0.49	0.63	Bal.
1.5Cr	0.33	3.13	1.51	0.48	0.60	Bal.
2.0Cr	0.31	2.93	1.98	0.53	0.57	Bal.
2.5Cr	0.27	2.87	2.46	0.53	0.59	Bal.

Nanomechanical tests

The nanomechanical properties of the boride were evaluated using a CSM Instruments nanoindenter (NANOVEA-NMT) equipped with a Berkovich-type diamond indenter. The typical load (P)–displacement (h) curve was obtained during the test by setting the maximum load as 80 mN, as shown in Fig. 1 [22–24]. Mechanical parameters, e.g. hardness (H) and elastic modulus (E), can be estimated from the P – h curves using Oliver and Pharr method [25, 26] and the following Eqs. (1), (2):

$$H = \frac{P_{\max}}{A_c} \tag{1}$$

$$\frac{1}{E_r} = \frac{1 - \nu^2}{E} + \frac{1 - \nu_i^2}{E_i} \tag{2}$$

where P_{\max} is the maximum load; A_c is the projected contact area between the indenter and specimen; E_r is the reduced Young’s modulus of the specimen; E and E_i , and ν and ν_i denote the Young’s modulus and Poisson’s ratio for the specimen and the indenter, respectively. For diamond indenter tip, $E_i = 1141$ - GPa and $\nu_i = 0.07$ [23, 26]. For Fe_2B crystal in this work, Poisson’s ratio $\nu = 0.388$ [27]. To minimize the experimental errors, the ultimate value of hardness and modulus was determined by averaging at least five examinations, respectively.

First-principles calculation

The first-principles calculation was carried out based on density functional theory. Ultrasoft pseudopotentials were used to describe the interactions of ionic

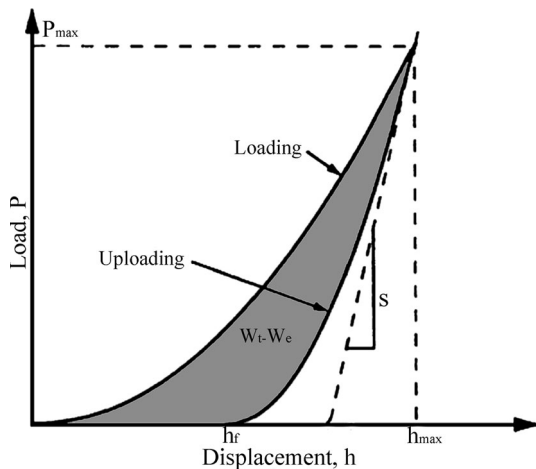


Figure 1 A typical load–displacement curve.

core and valence electrons. Generalized gradient approximation (GGA) within PBE scheme was employed to evaluate exchange–correlation energy. A special k point sampling method proposed by Monkhorst–Pack was used for the energy integration in the first irreducible Brillouin zone [28], and the k point mesh was selected as $10 \times 10 \times 12$. The kinetic energy cutoff 400 eV was used for plane wave expansions in reciprocal space. BFGS optimization method was used to find the ground state of Fe_2B crystals in which both atom positions and lattice parameters were optimized simultaneously [27, 29]. Total energy changes were finally reduced less than 1.0×10^{-6} eV/atom, and Hellman–Feynman forces acting on atoms were converged less than 0.01 eV/Å.

Results and discussion

Effect of chromium on the microstructure of Fe-3.0B alloy and M_2B

Figure 2 shows the SEM micrographs of the as-cast Fe-3.0B alloy. From the figures, it can be clearly found that 0Cr sample is composed of ferrite, pearlite and M_2B (M representing for Fe or Cr) with various morphologies, e.g. typical fish-like, net-like M_2B , rod-like M_2B and cluster-like M_2B . For 2Cr sample, only M_2B and typical pearlite matrix appear in the view. By comparison, we can find that M_2B grain tends to become visually coarse after chromium addition in Fe-3.0B alloy. In addition, ferrite in the metallic matrix gradually disappears with increasing the chromium addition. Considering the considerable hardenability of chromium, it is not difficult to understand the phenomenon of matrix phase transformation. During the solidification and cooling process, the continuous cooling transformation curve tends to move right after chromium addition, contributing to the improved hardenability of the alloy [30].

Volume fraction and morphology of M_2B have been quantitatively characterized in the current research. Beforehand, the five groups of alloys were heat-treated in order to distinguish M_2B from the matrix, which has been introduced elsewhere [12]. Equipped with optical microscope, a digital photograph processing software (DT2000) was used to statistically analyze the morphology and volume fraction of M_2B , as shown in Table 2. According to

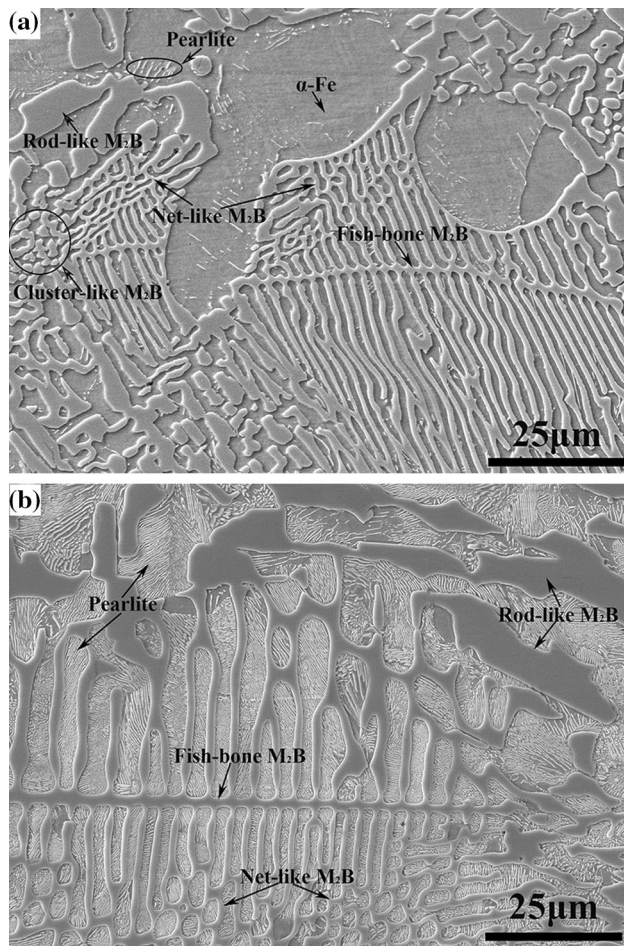


Figure 2 SEM micrographs of the as-cast microstructure of Fe-3.0B alloys: **a** 0Cr; **b** 2.0Cr.

Table 2 Volume fraction of M_2B in Fe-3.0B alloy (Vol%)

Sample	0Cr	1.0Cr	1.5Cr	2.0Cr	2.5Cr
Volume fraction of M_2B	22.37	22.24	23.65	22.19	22.07

the results, volume fraction of the boride fluctuates in an amplitude less than 1.58 vol% in all samples. In other words, chromium addition in Fe-3.0B alloy scarcely gives rise to a significant volume fraction variation of the boride. The result agrees well with previous report that the volume of boride is mainly affected by boron content in the alloy.

Figure 3 presents the grain size histograms of M_2B for all samples. The number density of fine borides (the equivalent cycle diameter less than 5 μm) firstly increases and then decreases with the increase in chromium addition while the area fraction of coarse

M_2B (the equivalent cycle diameter larger than 10 μm) has an opposite trend. Interestingly, the critical point for both variation trends locates on 2Cr sample. Accordingly, it can be deduced that chromium addition can hinder the continuous growth of M_2B crystal grain, leading to the increased number of fine borides. Furthermore, the average grain area of M_2B has been presented as a function of chromium content in Fig. 4. The average equivalent area (\AA) decreases firstly and then increases with the increase in chromium addition. Associating with the results in Fig. 3, it can be concluded that the variation of coarse M_2B plays a key role in affecting the average grain size of M_2B . However, the grain size variation is not very significant, with the largest difference not exceeding 7 μm^2 . Generally, the effect of chromium on grain size of M_2B may be against some previous views. In the previous studies, chromium addition was deemed to be able to refine the structure of carbides and pearlite in Fe-C alloy [31–33]. Besides, Zhang [18] found that the morphology of the boride would become less continuous with chromium addition of 17.94 wt%. However, a common ground in these studies is that the chromium content is considerably high. Thus, some Cr-C compounds and Cr-B compounds may be precipitated in advance during the solidification and act as an initial crystal nucleus, contributing to the refinement of crystal grains.

The morphology of M_2B has also been quantitatively characterized by a fractal dimension (D_f). In some cases, D_f can be generally used to characterize the morphology of the second phase, such as carbide and graphite [30, 34, 35]. The fractal dimension can be calculated by area-perimeter method [34], as shown in Eq. (3):

$$D_f = 2 \lg L_p / \lg A \quad (3)$$

where A and L_p is the area and the perimeter of borides, respectively.

As shown in Fig. 4, the fractal dimension of M_2B rises firstly and then drops with the increment of chromium content, which is somewhat opposite to trend of the average grain size. The result is exactly accordant to the empirical view that fractal dimension has an opposite trend to the grain size [36]. On the other hand, the variation of D_f is approximately opposite to that of coarse M_2B in Fig. 3. So we can deduce that coarse M_2B has an important influence on the fractal dimension (D_f). In general, the morphology tends to be globular as the fractal dimension

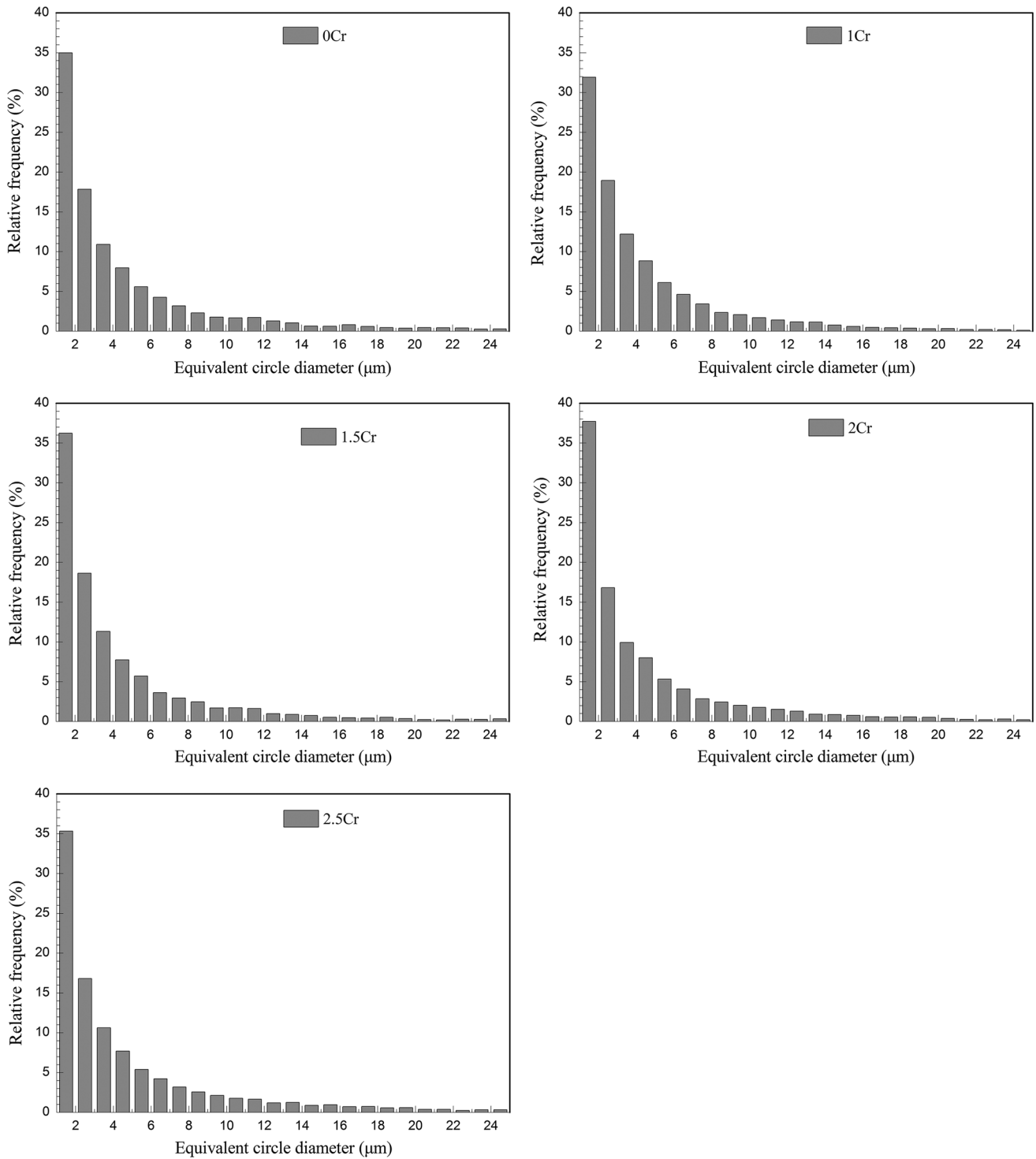


Figure 3 Distribution histograms of the equivalent circle diameter of the borides in Fe-3.0B alloys with different chromium contents.

(D_p) is close to 1 and vice versa. In this context, we can conclude that M_2B grain may gradually change from slender-type to wide-block feature with chromium

addition increasing from 1.0 to 2.5 wt%. Interestingly, this conclusion agrees well with the phenomenon of increasing coarse M_2B in return.

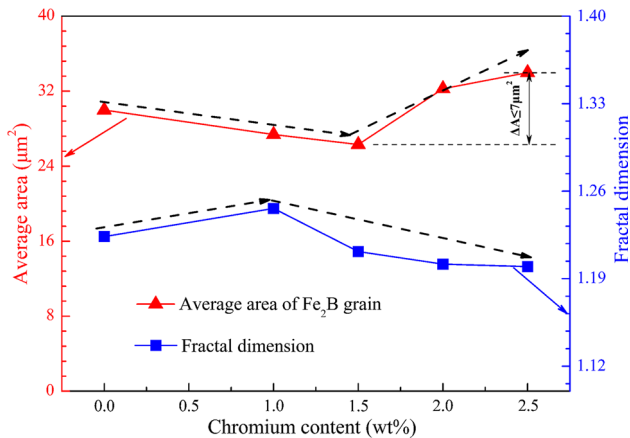


Figure 4 Average grain area and fractal dimension of the borides in Fe-3.0B alloys with different chromium contents.

Mechanical properties of M₂B

Nanoindentation tests have been conducted on M₂B grain to explore the effect of chromium on the mechanical properties. Figure 5 presents the load (*P*)–displacement (*h*) curves during indentation for each sample. No apparent displacement bursts can be found on the loading curves, indicating that the crack propagation and indentation size effect (ISE) during indenting process are negligible. As depicted from the inset in Fig. 5, the indentation by Berkovich indenter locates within M₂B grain. According to Oliver–Pharr method [23–26, 37–40], the hardness and elastic modulus of M₂B can be obtained from the *P*–*h* curves. As shown in Fig. 6, nanoindentation hardness of M₂B varies slightly in an according order

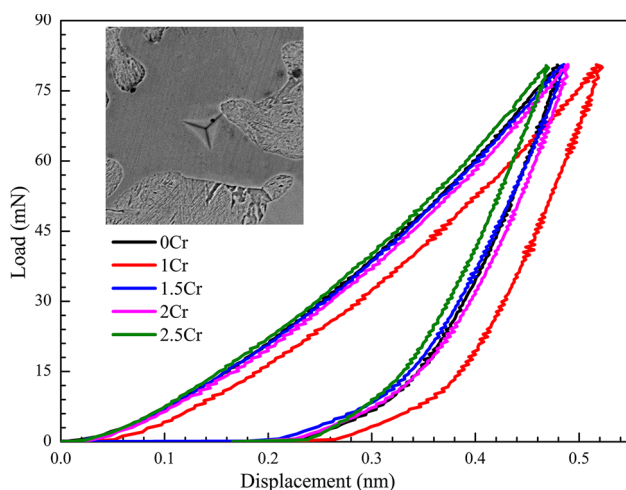


Figure 5 The load–displacement curves of the borides in Fe-3.0B alloys with different chromium contents.

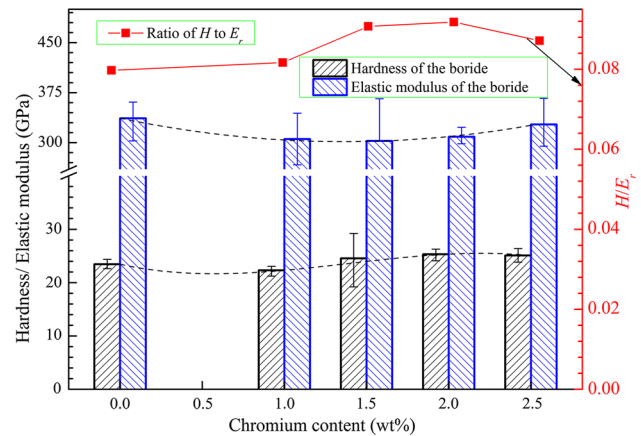


Fig. 6 Hardness, elastic modulus and H/E_r of the boride in Fe-3.0B alloys with different chromium contents.

of magnitude (near 24 GPa) with the increase in chromium content. Compared with previous results of Vickers hardness [9, 11–13], the nanoindentation hardness appears to be larger. Generally, the hardness of material is supposed to decrease with the increase in testing load, so the result of hardness in current research is reasonable. On the other hand, the elastic modulus of M₂B declines firstly and then increases slightly, within the range from 302.53 to 336.54 GPa. At chromium content of 1.5 wt%, the elastic modulus achieves its minimum value. And the evolution of elastic modulus of M₂B is in accordance with the results of the first-principles calculation [27].

Furthermore, the ratio of $H-E_r$ can be obtained accordingly. As shown in Fig. 6, H/E_r of M₂B increases firstly and then decreases, reaching the peak value of 0.092 at chromium content of 2.0 wt%. Previous studies have found that H/E_r owns an approximately linear relationship with W_e/W_t (W_e : the elastic work during the uploading process; W_t : the total work during the indentation test) [22, 24]. In this context, the higher the H/E_r of the boride, the higher the elastic recovery work. During the indentation process, elastic and plastic deformations simultaneously take place around and beneath the indenter. Unfortunately, M₂B is such a brittle intermetallic that microcracks are bound to arise along with the deformation. Accordingly, part of the total work during the indenting process will be consumed to support the surface energy originating from the occurrence of microcracks. Consequently, the elastic work (W_e) to support the elastic recovery during the uploading process will decline. The more severe the phenomenon of microcracks, the less the elastic work.

In other words, higher elastic work indicates better toughness of M_2B . In view of the linear relationship between H/E_r and elastic recovery, the H/E_r can reflect the toughness of the boride to some extent. Thereby, it can be concluded that the toughness of M_2B increases firstly and then decreases with increasing chromium content, obtaining the highest toughness at the chromium content of 2.0 wt%.

Toughening mechanism of chromium addition in M_2B

In the current work, the tetragonal Fe_2B with the $I4/MCM$ space group has been selected to conduct the first-principles calculations [41]. As for $(Fe, Cr)_2B$ crystal structure, one of Fe atoms in the initial Fe_2B crystal cell is replaced with one Cr atom. The crystal cells parameters and atomic positions have been fully optimized by performing the first-principles calculations. The lattice parameters of Fe_2B have been determined to be $a = b = 4.89 \text{ \AA}$ and $c = 4.222 \text{ \AA}$, while these of $(Fe, Cr)_2B$ to be $a = b = 4.986 \text{ \AA}$ and $c = 4.107 \text{ \AA}$. With Cr atom being doped, the crystal lattice of Fe_2B can be compressed in some degree along [002] direction and expanded a little transverse to [002] direction. In addition, population analysis results show that the average bond lengths of B–B are 2.11 and 1.94 \AA for Fe_2B and $(Fe, Cr)_2B$, respectively.

Table 3 shows the binding energy and mechanical modulus of Fe_2B and $(Fe, Cr)_2B$. It can be found that E_{binding} of M_2B decreases slightly from -105.934 to -106.976 eV/Cell , which indicates that $(Fe, Cr)_2B$ may be more thermodynamically stable than the initial Fe_2B . On the other hand, the elastic modulus of M_2B ranges from 326.934 to 350.007 GPa, which is according to the experimental results of nanoindentation in Fig. 6. Furthermore, the ratio of bulk modulus and shear modulus (B/G) increases slightly, which indicates the toughness of M_2B can be improved to some extent after Cr atom being doped [27].

Table 3 Binding energy and modulus of Fe_2B and $(Fe, Cr)_2B$

Species	Cell formula	Binding energy(eV/Cell)	Bulk modulus/B (Gpa)	Shear modulus/G (Gpa)	Elastic modulus (Gpa)	B/G
Fe_2B	Fe_8B_4	-105.934	305.767	123.670	326.934	2.47
$(Fe, Cr)_2B$	Fe_7CrB_4	-106.976	328.359	132.343	350.007	2.48

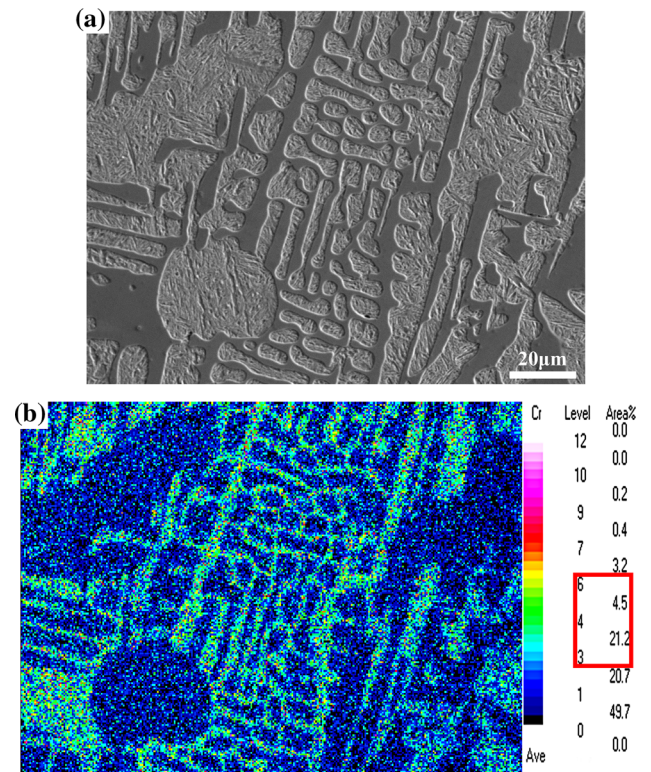


Figure 7 Chromium distribution in Fe-3.0B alloy: **a** Heat-treated microstructure of 2Cr, **b** Mapping of chromium distribution.

Figure 7 exhibits the EPMA mapping of chromium distribution in 2Cr sample. Chromium concentration in M_2B is evidently higher than the surrounding metallic matrix. According to Fig. 7b, the total area with chromium concentration ranging from 3.0 to 6.0 wt% reaches about 25.7 area %, which is approximately equal to the volume fraction of M_2B in 2Cr sample. In this case, we can conclude that chromium tends to segregate in M_2B after being added in Fe-3.0B alloy. A number of factors can be supposed to contribute to the segregation phenomenon. Firstly, due to the similar atom radius and electronegativity, iron atom in M_2B can be effectively replaced by chromium. On the other hand, during solidification solute atoms are partitioned between the solid phase (S) and liquid phase (L) to either enrich or deplete

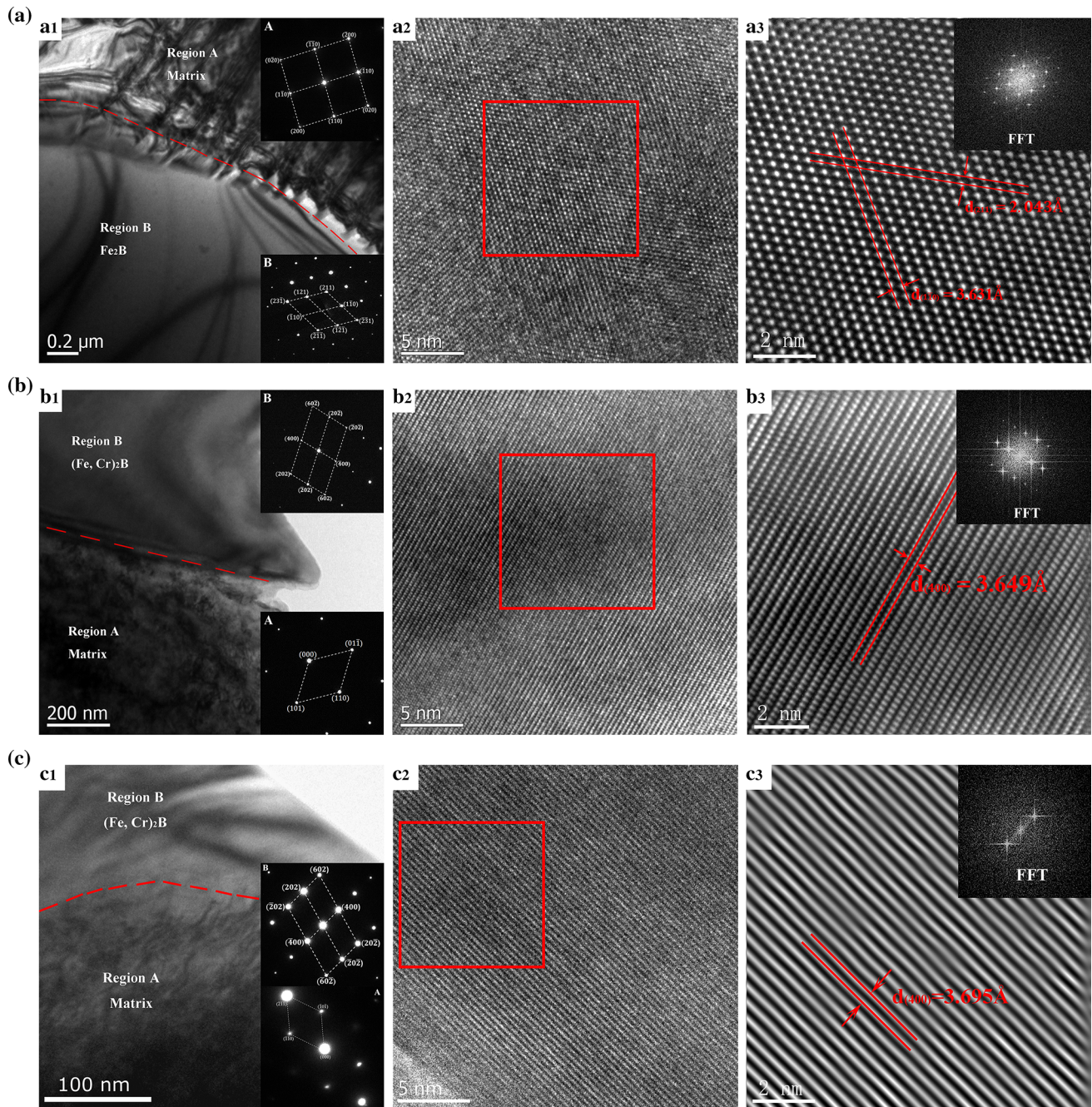


Figure 8 HRTEM micrographs of the boride in 0Cr **a**, 1Cr **b** and 2Cr **c** sample: **a1–c1** bright-field images and the SADPs; **a2–c2** high-magnified micrographs of the boride; **a3–c3** inverse Fourier-filtered images of the boride.

region depending on the solute atom partition coefficient ($K = C_S/C_L$, where C_S and C_L are defined as the solute concentration in the S and L, respectively). With the partition coefficient being less than 1, chromium tends to segregate in the liquid contributing to a higher chromium content in the final liquid before eutectic reaction. Furthermore, chromium has strong affinity with boron, which also

contributes to the chromium concentration in boride being higher than the matrix. From the comparison of the binding energy of M_2B in Table 3, the possibility of chromium replacement can be explained thermodynamically. Taking all the factors above into consideration, it is reasonable for the segregation of chromium in M_2B .

Figure 8 shows the results of high-resolution transmission electron microscope (HRTEM) observation for 0Cr, 1Cr and 2Cr samples, respectively. Figure 8a1–c1 is the bright-field images combining with the corresponding selected area diffraction patterns (SADP) of 0Cr, 1Cr and 2Cr, respectively. For all samples, Fe-3.0B alloy is composed of smooth boride and rough metallic matrix. The matrix has been identified as martensite due to its typical body-centered cubic patterns in designated region A. For 0Cr sample, the SADP of M_2B can be identified as the tetragonal lattice, revealing the typical lattice structure of Fe_2B (indexed by ICSD#42530). From high-magnified micrograph of M_2B in Fig. 8a2, the atomic arrangement is quite orderliness and no evident defects (e.g. dislocations, stacking faults) appear, which may be attributed to the considerable stiffness and elastic modulus of hard Fe_2B . From the inverse Fourier-filtered (IFFT) image in Fig. 8a3, the crystal plane spacings of (211) and (110) can be measured to be 2.043 and 3.631 Å, respectively, according to the standard spacings of 2.013 and 3.613 Å. However, for 1 and 2Cr samples, M_2B can be identified as the orthorhombic lattice structure, revealing to be $(Fe, Cr)_2B$ (indexed by ICSD#16554). From the IFFT images in Fig. 8b3 and c3, the spacings of (400) plane for 1 and 2Cr sample are 3.649 and 3.695 Å, respectively, being approximately equal to the theoretical value of 3.643 Å within the range of accidental error. Therefore, it can be concluded that the crystal lattice of Fe_2B may transform from tetragonal to orthorhombic ($(Fe, Cr)_2B$) lattice with chromium addition.

According to the first-principles calculation result, with fully structure optimization, the crystal lattice of M_2B transforms from tetragonal (Fe_3B_4) to orthorhombic structure (Fe_7CrB_4) after chromium doped. This result is exactly accordant to the above experimental data. Furthermore, the initial B–B bond length along [002] has been shorted by about 8% as a result of the lattice evolution of M_2B . Therefore, the inherently weak B–B bond is expected to be strengthened accordingly. In this context, the fracture toughness of Fe_2B is supposed to be improved with the weakest chain being reinforced.

However, if the chromium addition exceeds the ideal limit, excessive chromium may dissolve into M_2B generating excessive $(Fe, Cr)_2B$ crystal cell. In this case, large amounts of distorted cells (orthorhombic structure) will cause considerable

defects in the whole M_2B grain. In reverse, fracture toughness of the boride may turn to decrease. In this context, the decline of fracture toughness of M_2B in 2.5Cr sample can be explained reasonably. In conclusion, appropriate chromium addition can help improve the fracture toughness of M_2B by affecting the crystal lattice and strengthening the weak bond.

Conclusions

The morphology, mechanical properties and crystal lattice structure of M_2B in Fe-3.0B alloys with different chromium additions have been investigated. The following conclusions can be drawn:

- (1) With increasing chromium addition, the average grain size of M_2B (Å) decreases firstly and then increases slightly, while the fractal dimension (D_f) has an opposite trend.
- (2) The hardness of M_2B changes little while the elastic modulus decreases firstly and then increases with the increase in chromium addition; H/E_r increases firstly and then decreases and reaches the maximum value at chromium addition of 2.0 wt%.
- (3) With chromium addition, M_2B crystal tends to be more thermodynamically stable with the binding energy decreasing from -105.934 to -106.976 eV/cell; the elastic modulus and B/G can also be improved.
- (4) With chromium addition, the crystal lattice of Fe_2B may transform from tetragonal to orthorhombic structure ($(Fe, Cr)_2B$), contributing to shortening the length of B–B bond along [002] direction.

Acknowledgements

Yongxin Jian thanks to Zhifu Huang, Jiandong Xing and Yimin Gao for their good advice. This work was supported by the National Natural Science Foundations of China (Grant No: 51371138 and 51571159), the Science and Technology Project of Guangdong Province in China (2015B090926009) and the Science and Technology Project of Guangzhou City in China (201604046009).

Compliance with ethical standards

Conflict of interest The authors declared that they have no conflicts of interest to this work. We declare that we do not have any commercial or associative interest that represents a conflict of interest in connection with the work submitted.

References

- [1] Çetinkaya C (2006) *Mater Des* 27:437–445. <https://doi.org/10.1016/j.matdes.2004.11.021>
- [2] Chen KM, Zhou Y, Li XX, Zhang QY, Wang L, Wang SQ (2015) *Mater Des* 65:65–78. <https://doi.org/10.1016/j.matdes.2014.09.016>
- [3] Yasir M, Zhang C, Wang W, Xu P, Liu L (2015) *Mater Des* 88:207–213. <https://doi.org/10.1016/j.matdes.2015.08.142>
- [4] Zhou Y, Zhang QY, Liu JQ, Cui XH, Mo JG, Wang SQ (2015) *Wear* 344–345:9–21. <https://doi.org/10.1016/j.wear.2015.10.015>
- [5] Xu X, van der Zwaag S, Xu W (2016) *Wear* 348–349:80–88. <https://doi.org/10.1016/j.wear.2015.11.017>
- [6] Zambrano OA, Aguilar Y, Valdés J, Rodríguez SA, Coronado JJ (2016) *Wear* 348–349:61–68. <https://doi.org/10.1016/j.wear.2015.11.019>
- [7] Zhang N, Zhang J, Lu L, Zhang M, Zeng D, Song Q (2016) *Mater Des* 89:815–822. <https://doi.org/10.1016/j.matdes.2015.10.037>
- [8] ASM International Alloy Phase Diagram and the Handbook Committees (1992) ASM handbook, volume 3: alloy phase diagrams. ASM International, Materials Park, OH
- [9] Jian Y, Huang Z, Xing J, Guo X, Jiang K (2017) *J Mater Res*. <https://doi.org/10.1557/jmr.2017.41>
- [10] Jian Y, Huang Z, Xing J, Li J (2017) *Wear* 378–379:165–173. <https://doi.org/10.1016/j.wear.2017.02.042>
- [11] Jian Y, Huang Z, Xing J, Guo X, Wang Y, Lv Z (2016) *Tribol Int* 103:243–251. <https://doi.org/10.1016/j.triboint.2016.07.008>
- [12] Jian Y, Huang Z, Xing J et al (2016) *Wear* 362–363:68–77. <https://doi.org/10.1016/j.wear.2016.04.029>
- [13] Jian Y, Huang Z, Xing J, Wang B (2015) *Mater Charact* 110:138–144. <https://doi.org/10.1016/j.matchar.2015.10.017>
- [14] Lv Z, Fu H, Xing J, Huang Z, Ma S, Hu Y (2016) *Corros Sci* 108:185–193. <https://doi.org/10.1016/j.corsci.2016.03.002>
- [15] Lv Z, Fu H, Xing J, Ma S, Hu Y (2016) *J Alloy Compd* 662:54–62. <https://doi.org/10.1016/j.jallcom.2015.11.171>
- [16] Wang Y, Xing J, Ma S et al (2015) *Corros Sci* 98:240–248. <https://doi.org/10.1016/j.corsci.2015.05.039>
- [17] Ma S, Xing J, He Y, Fu H, Li Y, Liu G (2016) *Acta Mater* 115:392–402. <https://doi.org/10.1016/j.actamat.2016.06.016>
- [18] Zhang J, Gao Y, Xing J, Ma S, Yi D, Yan J (2011) *Tribol Lett* 44:31–39. <https://doi.org/10.1007/s11249-011-9823-5>
- [19] Yi D, Xing J, Ma S et al (2011) *Tribol Lett* 45:427–435. <https://doi.org/10.1007/s11249-011-9900-9>
- [20] Lentz J, Röttger A, Theisen W (2015) *Acta Mater* 99:119–129
- [21] Musen L, Shaoli F, Wandong X, Ruihuang ZRY (1995) *Acta Metall Sin* 31:201–207
- [22] Frutos E, González-Carrasco JL (2013) *Acta Mater* 61:1886–1894. <https://doi.org/10.1016/j.actamat.2012.12.009>
- [23] Jian S-R, Chen G-J, Hsu W-M (2013) *Materials* 6:4505–4513. <https://doi.org/10.3390/ma6104505>
- [24] Zhang T, Feng Y, Yang R, Jiang P (2010) *Scripta Mater* 62:199–201. <https://doi.org/10.1016/j.scriptamat.2009.10.025>
- [25] Oliver WC, Pharr GM (1992) *J Mater Res* 7:1564–1583
- [26] Li X, Bhushan B (2002) *Mater Charact* 48:11–36
- [27] Xiao B, Feng J, Zhou CT et al (2010) *Physica B* 405:1274–1278. <https://doi.org/10.1016/j.physb.2009.11.064>
- [28] Monkhorst HJ, Pack JD (1976) *Phys Rev B* 13:5188–5192
- [29] Xiao B, Xing JD, Ding SF, Su W (2008) *Physica B* 403:1723–1730. <https://doi.org/10.1016/j.physb.2007.10.014>
- [30] W Lu, L Li, L Huang (2002) China Machine Press, Beijing
- [31] Scandian C, Boher C, de Mello JDB, Rézai-Aria F (2009) *Wear* 267:401–408. <https://doi.org/10.1016/j.wear.2008.12.095>
- [32] H Chen, J Xing, W Li (2006) China Machine Press, Beijing
- [33] Q Zhou (1986) Xi'an Jiaotong University Press, Xi'an: 18
- [34] BB Mandelbrot, DE Passoja, AJ Paullay (1984)
- [35] Radulovic M, Fiset M, Peev K, Tomovic M (1994) *Journal of Materials Science* 29:5085–5094. <https://doi.org/10.1023/B:JMSE.0000007730.00517.65>
- [36] Zhou J, WANG Y, LIU Z (2000) *J East China Univ Sci Technol* 26:188–190
- [37] Anstis PCGR, Lawn BR, Marshall DB (1981) *J Am Ceram Soc* 64:533–538
- [38] Mukhopadhyay NK, Belger A, Paufler P, Kim DH (2007) *Mater Sci Eng A* 449–451:954–957. <https://doi.org/10.1016/j.msea.2006.02.258>
- [39] Ozmetin AE, Sahin O, Ongun E, Kuru M (2015) *J Alloy Compd* 619:262–266. <https://doi.org/10.1016/j.jallcom.2014.09.015>
- [40] Vincent S, Murty BS, Kramer MJ, Bhatt J (2015) *Mater Des* 65:98–103. <https://doi.org/10.1016/j.matdes.2014.09.017>
- [41] Havinga E, Damsma H, Hokkeling P (1972) *J Less Common Metals* 27:169–186